*Article*

# Co and Ni Incorporated γ-Al$_2$O$_3$ (110) Surface: A Density Functional Theory Study

Huaxi Li [1,2], Liu Shi [3,*], Chengkai Jin [1], Runping Ye [1] and Rongbin Zhang [1,*]

[1]  Key Laboratory of Jiangxi Province for Environment and Energy Catalysis, Institute of Applied Chemistry, College of Chemistry, Nanchang University, No. 999 Xuefu Road, Nanchang 330031, China; lihxjxak@163.com (H.L.); jinck1998@163.com (C.J.); rye@ncu.edu.cn (R.Y.)

[2]  The Laboratory of the Emergency Management Technical Support Center, Jiangxi Academy of Emergency Management Science, No. 999 Wugong Mountain Road, Nanchang 330103, China

[3]  State Key Laboratory of Coal Combustion, School of Energy and Power Engineering, Huazhong University of Science and Technology, No. 1037 Luoyu Road, Wuhan 430074, China

*  Correspondence: liu_shi@hust.edu.cn (L.S.); rbzhang@ncu.edu.cn (R.Z.)

**Abstract:** Investigation into the state and mechanisms of the active metal substitution into the γ-Al$_2$O$_3$ support is the basis for design of many catalysts. Periodic density functional theory (DFT) +U calculations were used to investigate the surface properties of transition metals Co$^{3+}$ and Ni$^{3+}$ cations substitute for the Al$^{3+}$ cations of γ-Al$_2$O$_3$ (110) surface. It was found that the substitution energy of one Al$^{3+}$ substituted by Co$^{3+}$ and Ni$^{3+}$ are −61 and −57 kJ/mol, respectively. The Co and Ni preferentially substitute the tetrahedral Al sites instead of the octahedral Al sites. Using thermodynamics, the Al atoms in the top layer of γ-Al$_2$O$_3$ (110) can be 100% substituted by Co and Ni. Ni is easier to substitute the Al atom than Co. There is no obvious structural distortion that occurs after Co and Ni substituted all the top layer Al atoms. While the band gaps of the substituted surface become narrower, resulting in the increase of surface Lewis acidity. In addition, the oxygen vacancy formation energies of the Co and Ni substituted surface are 268 and 53 kJ/mol, respectively. The results provide interface structure and physical chemistry properties of metal-doped catalysts.

**Keywords:** γ-Al$_2$O$_3$; transition metal; substitution; surface property; DFT

## 1. Introduction

γ-Al$_2$O$_3$ is commonly used as a catalyst support, due to its performance and excellent thermal stability, good adsorption and high specific surface area [1]. Transition metal substitution into γ-Al$_2$O$_3$ surface to form high-performance catalyst is widely used in the industrial field. Co$^{3+}$ and Ni$^{3+}$ cations are of interest to researchers because they are isovalent with Al$^{3+}$ and can form stable oxides. More importantly, the Co doped γ-Al$_2$O$_3$ exhibits excellent catalytic activity in Fischer–Tropsch synthesis [2–5] vs. Ni doped γ-Al$_2$O$_3$ applied in hydrogenation [6,7], dehydrogenation reaction [8] and alcohol steam reforming reaction [9,10].

The properties of Co and Ni substituted γ-Al$_2$O$_3$ surfaces have been studied in previous experiments [11–13]. Some characterization techniques were applied to explore the Co and Ni substituted γ-Al$_2$O$_3$ surfaces properties, such as X-ray diffraction (XRD) [14,15], CO$_2$ temperature programmed desorption (CO$_2$-TPD) [14], and H$_2$-temperature programmed reduction (H$_2$-TPR) [16,17]. Jaroniec et al. [14] synthesized 10% of Co and Ni added into γ-Al$_2$O$_3$, they found the peaks of Co$_3$O$_4$, Ni$_2$O$_3$ and NiO in the XRD patterns. The Co$_3$O$_4$, Ni$_2$O$_3$ and NiO peaks disappeared when the temperature was higher than 823 K. Laine et al. [18] used the XRD and assumed that the Co substituted for the tetragonal site Al atoms. In addition, the phase diagrams showed that the structure of Ni/γ-Al$_2$O$_3$ and Co/γ-Al$_2$O$_3$ changed with the temperature and doped metal content [19,20]. The CO$_2$-TPD results [14] detects that the doped Ni and Co enhanced acid-base properties of catalyst surface.

Using the first principal method to study the surface properties of doped catalysts is of interest to researchers [21–27]. Gu et al. [28] studied the surface properties of the Fe doped $\gamma$-Al$_2$O$_3$(111) surface. They found that the Me-O (Me indicates the transition metal atom) bond distances were increased after substitution reaction. Furthermore, the surface charge is redistributed, with part of Fe atoms only as electron acceptor, and the others Fe atoms as electron donor and acceptor. Benam et al. [29] studied the band gap of the IIIB transition metal substituted $\alpha$-Al$_2$O$_3$ unit cell, and it was found that the bond gap became narrower with the ionic radius increase, as the order of 3d < 4d < 5d < 6d. Baltrusaitis et al. [30] found the Me-O bond distances of the Fe and Cr doped $\alpha$-Al$_2$O$_3$(0001) surface had no obvious change. The empty Fe and Cr 3$d$ orbitals increased after substitution, which changed the surface charge properties, resulting in different adsorption properties for CO. The surface properties of other metal-doped supports have also been studied. Pacchioni et al. [31] used DFT-GGA method to study the boron(B)-doped anatase TiO$_2$, and they found two kinds of B structures of neutral and diamagnetic, which proved the two different XPS signals of B. Gu et al. [32] found the dopants of In and Sb could form stable geometries with the graphene. Yan [27] analyzed surface electronic structure of Ru/TiO$_2$(101) surface, they found that the electrons were transferred from the Ru active metal to the TiO$_2$ (101) support surface. Wang [33] reported that the clean and hydroxylation Pt$_4$/$\gamma$-Al$_2$O$_3$ (110) surfaces exhibited different catalytic performances for CO$_2$ hydrogenation, and the hydroxyl could weakness the interaction between Pt$_4$ and $\gamma$-Al$_2$O$_3$ (110) surface. Zhang [34] studied the Ag atom doped into the hydroxylated $\gamma$-Al$_2$O$_3$ (110) and (100) surfaces, they found that the terminal hydroxyl groups bond and disperse the Ag active metal, which lead the Ag/nano-Al$_2$O$_3$ had high catalytic performance in HC-SCR of NO.

Our previous work [35] has used DFT+U method to investigate the Cu$^{2+}$ substitution into the $\gamma$-Al$_2$O$_3$ (100) and (110) surfaces. The results show that the substitution energies of one Cu$^{2+}$ and H$^+$ substitution for $\gamma$-Al$_2$O$_3$ (100) and (110) surfaces were $-120$ and $-261$ kJ/mol, respectively. In addition, the substituted Cu atoms had better selectivity to the surface tetrahedral Al sites. The surface Al could be 100% substitution by Cu to form spinel-like structure, which was agreed well with experimental results. Moreover, the Fe, Co and Ni doped into the CuAl$_2$O$_4$ spinel surfaces were also studied [25]. The substitution energies of Me$^{3+}$ cations substitution for tetrahedral Al$^{3+}$ cations were in the order of Fe > Co > Ni; vs. Ni > Co > Fe for octahedral Al$^{3+}$ cations.

In conclusion, the Co and Ni doped $\gamma$-Al$_2$O$_3$ exhibits excellent catalytic activity in industrial field. However, conventional experimental research usually focus on the catalytic performance, while the molecular level insights for the understanding of the interface structures and physical chemistry properties of Co and Ni substituted $\gamma$-Al$_2$O$_3$ are still not clear. It was reported that the active metals of Ni and Co were mainly doped into the most stable $\gamma$-Al$_2$O$_3$ surfaces (e.g., (110) [36], (220) [37] and (440) [38–40] surfaces in XRD pattern). Meanwhile, the theoretical calculations reported by Digne et al. showed that the $\gamma$-Al$_2$O$_3$ (110) surface dominates largely 74% of the total surface area of $\gamma$-Al$_2$O$_3$ surface [41,42]. This model agrees well with the experimental data i.e., bulk modulus, XRD, NMR, electronic density and the acid–base surface properties [43,44]. In addition, the $\gamma$-Al$_2$O$_3$ model has been widely used in related research of $\gamma$-Al$_2$O$_3$, such as Ag/$\gamma$-Al$_2$O$_3$ [34], Rh/$\gamma$-Al$_2$O$_3$ [45], Pd/$\gamma$-Al$_2$O$_3$ [33], Pt/$\gamma$-Al$_2$O$_3$ [46] and Fe doped $\gamma$-Al$_2$O$_3$ [28,47]. Investigation into the Ni and Co doped $\gamma$-Al$_2$O$_3$ (110) surface could provide interface structure and physical chemistry properties of Ni and Co doped $\gamma$-Al$_2$O$_3$ catalysts.

The present work was aimed to investigate the surfaces structures of the Co and Ni substitution into the $\gamma$-Al$_2$O$_3$ (110) surface. The surface charge properties, substitution mechanism by the projected density of states (PDOS), and surface stability via oxygen vacancy were analyzed.

## 2. Results and Discussion

### 2.1. Substitution of $Al^{3+}$ by $Co^{3+}$ and $Ni^{3+}$

#### 2.1.1. Substitution of $Al^{3+}$ by $Co^{3+}$

Figure 1 shows the structures of the $Co^{3+}$ cations substituted $\gamma$-$Al_2O_3$ (110) surface. The results show that the most favorable substitution structure of one Co substituted $\gamma$-$Al_2O_3$ (110) surface is (110)-1Co-4, with the substitution reaction exothermic by $-61$ kJ/mol. The electronic structure of Co changes after substitution. The Bader charge of substituted $Co(4)_{3c}$ is $+1.40$ e, which is smaller than the $Al(4)_{3c}$ cation ($+2.38$ e) of the perfect $\gamma$-$Al_2O_3$ (110) surface. The substituted $Co(4)_{3c}$ atom bonds with the $O(5)_{2c}$, $O(6)_{2c}$ and $O(sublayer)_{4c}$ with the Co-O bond distances of 183, 183 and 196 pm, respectively, which are longer than the Al(4)-O bond distances (171, 171 and 179 pm) of the perfect $\gamma$-$Al_2O_3$ (110) surface. It agrees well that the covalent radius of Co (126 pm) is larger than Al (121 pm) [48]. For the substitution of $Al(1)_{4c}$ and $Al(3)_{4c}$ by Co atom, the substitution energies are 26 and $-29$ kJ/mol, respectively. It is worth noting that the $Al(4)_{3c}$ site is tetrahedral structure, and the $Al(1,2,4)_{4c}$ sites are octahedral structure. It means that Co atoms are easier to substitution the $\gamma$-$Al_2O_3$ (110) surface tetrahedral Al atoms than the octahedral Al atoms. In addition, the substitution of sublayer $Al(5)_{3c}$ by Co is also calculated, with the substitution energy endothermic of 82 kJ/mol, which is thermodynamically unfavorable. This indicates that Co preferentially substitution surface Al sites rather than subsurface Al sites.
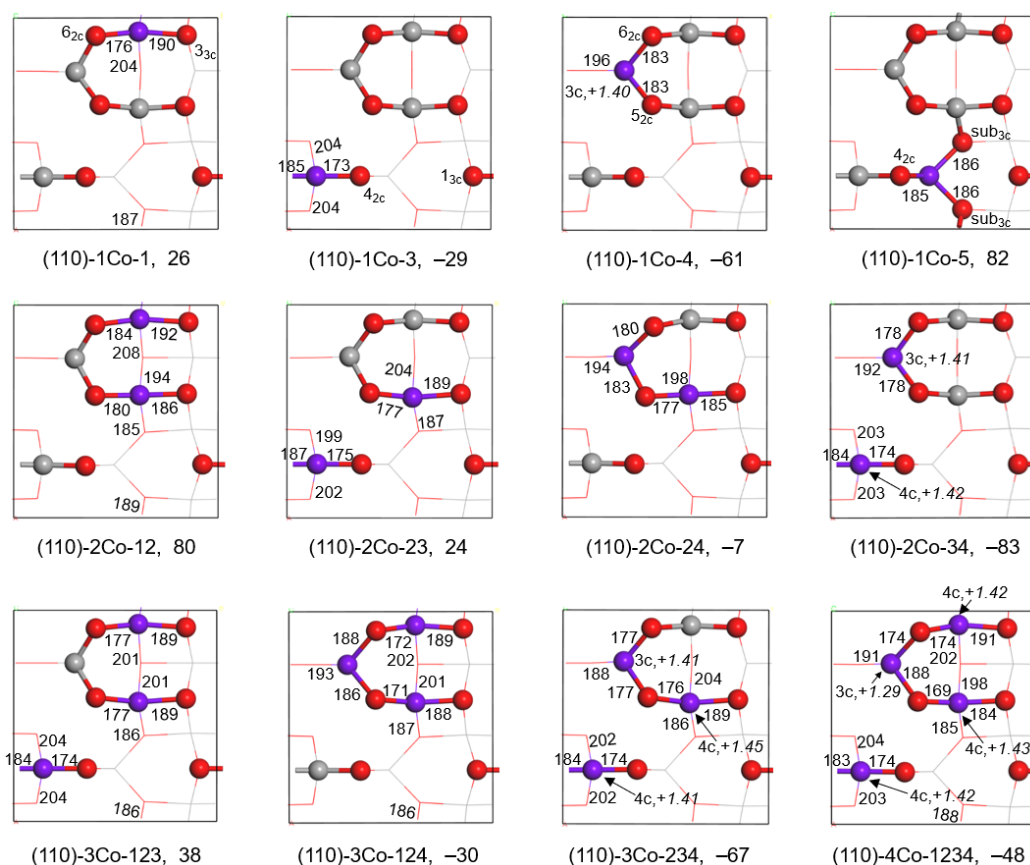


**Figure 1.** $Co^{3+}$ cations substituted for 1~4 $Al^{3+}$ cations of $\gamma$-$Al_2O_3$ (110) surface. The red, gray and violet balls represent the surface O, Al and Co atoms, respectively. The coordination numbers and Bader charges of Co atoms are next to the violet balls. The substitution energies (kJ/mol), Bader charges (*e*) and bond distances (pm) have been shown in the figure.

For two $Co^{3+}$ cations substitution for $Al^{3+}$ cations of γ-$Al_2O_3$ (110) surface. The substitution energies of (110)-2Co-12, (110)-2Co-23, (110)-2Co-24 and (110)-2Co-34 are 80, 24, −7 and −83 kJ/mol, respectively. It indicates that the substitution reaction is thermodynamically favorable at Al(2,4) and Al(3,4) sites, besides, the most thermodynamics favorable substitution structure is (110)-2Co-34. For the (110)-2Co-34 structure, the Bader charge of Co(3,4) are +1.42 and +1.41 e, and the average bond distances are 183 and 191 pm, respectively. For three $Co^{3+}$ cations substitution for the $Al^{3+}$ cations of γ-$Al_2O_3$ (110) surface. The substitution energies for (110)-3Co-123, (110)-3Co-124 and (110)-3Co-234 are 38, −30 and −67 kJ/mol, respectively. The most thermodynamics favorable substitution site is Al(2,3,4). For the (110)-3Co-234 structure, the Bader charge of Co(2,3,4) are +1.45, +1.41 and +1.41 e vs. 189, 181 and 191 pm for the average bond distances, respectively.

For $Co^{3+}$ cations completely substitute the $Al^{3+}$ cations top layer of γ-$Al_2O_3$ (110) surface, the substitution reaction of (110)-4Co-1234 structure is exothermic by −48 kJ/mol. It indicates that the $Co^{3+}$ completely substituted all the top layer $Al^{3+}$ cations are thermodynamically favorable. In the (110)-4Co-1234 structure, the Co(4)$_{3c}$ atom is in the tetrahedral position vs. the Co(1,2,3)$_{4c}$ atoms is in the octahedral position. In addition, after $Co^{3+}$ substitution for the surface Al atoms, there is no large surface structure change, which is consistent with the Fe and Cr substituted for the α-$Al_2O_3$(0001) surface Al atoms [30].

2.1.2. Substitution of $Al^{3+}$ by $Ni^{3+}$

Figure 2 shows the structures of the $Ni^{3+}$ cations substituted γ-$Al_2O_3$ (110) surface. The results present that the most favorable substitution structure of one $Ni^{3+}$ cation substituted the γ-$Al_2O_3$ (110) surface is (110)-1Ni-4, with exothermic of −61 kJ/mol. The substitution energy of (110)-1Ni-4 is slightly smaller than the (110)-1Co-4 by 4 kJ/mol. The surface electronic structure is redistributed after the $Ni^{3+}$ cations substitution. The Bader charge of Ni(4)$_{3c}$ is +1.22 e, which is slightly smaller to the doped Co of (110)-1Co-4 structure (+1.40 e). In addition, the structure of (110)-1Ni-4 is similar to the (110)-1Co-4. The substituted Ni atom bonds with two top layer O(5), O(6) atoms and one sublayer O atom, with the bond distances of 178, 178 and 195 pm, respectively. The Ni-O bond distances are slightly shorter than the Co-O, while it is longer than the Al-O bond distances. It is reported that the covalent radius of Ni is 124 pm [48]. The substitution energy for one $Ni^{3+}$ cation substitutes Al(1)$_{4c}$ cation is 18 kJ/mol vs. −18 kJ/mol for the Al(3)$_{4c}$ site. In addition, the $Ni^{3+}$ substitution of sublayer Al(5)$_{3c}$ atom is thermodynamically unfavorable.

It is interesting that the substitution properties of $Ni^{3+}$ cations into γ-$Al_2O_3$ (110) surface are similar to the $Co^{3+}$ cations. The Co and Ni atoms preferentially substitute for the tetrahedral Al sites rather than the octahedral Al sites, which consistent with previously reported experiments [18,49,50]. In additon, Co and Ni atoms preferentially substitute for the top layer Al sites rather than the sublayer Al sites.

For two $Ni^{3+}$ cations substitution for $Al^{3+}$ cations of γ-$Al_2O_3$ (110) surface, the substitution energies of (110)-2Ni-12, (110)-2Ni-23, (110)-2Ni-24 and (110)-2Ni-34 are 31, −1, −79 and −91 kJ/mol. It suggests that only the doping sites of Al(1,2) is thermodynamics unfavorable. For the most thermodynamics favorable substitution structure of (110)-2Ni-34, the Bader charge for Ni(3,4) is +1.25 and +1.15 e vs. 187 and 186 pm for the average bond distances, respectively. For three $Ni^{3+}$ cations substitution for $Al^{3+}$ cations of γ-$Al_2O_3$ (110) surface, the substitution energies of (110)-3Ni-123, (110)-3Ni-124 and (110)-3Ni-234 are −17, −79 and −96 kJ/mol. It can be found that the substitution reactions of three $Ni^{3+}$ are thermodynamically favorable. For the most thermodynamics favorable substitution structure of (110)-3Ni-234, the Bader charge for Ni(2,3,4) is +1.22, +1.28 and +1.28 e vs. 185, 188 and 185 pm for the average bond distances, respectively.
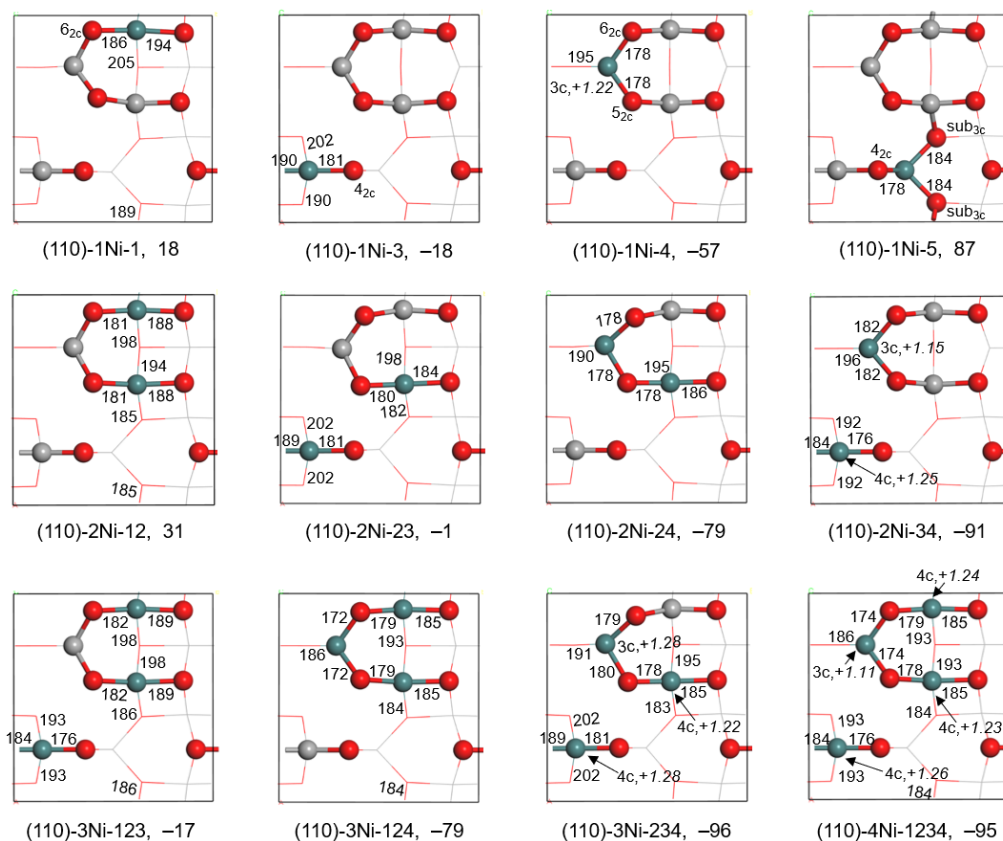
**Figure 2.** Ni$^{3+}$ substituted for 1~4 Al$^{3+}$ of $\gamma$-Al$_2$O$_3$ (110) surface. The red, gray and olive-green balls represent the surface O, Al and Ni atoms, respectively. The coordination numbers and Bader charges of Ni atoms are next to the olive-green balls. The substitution energies (kJ/mol), Bader charges (*e*) and bond distances (pm) have been shown in the figure.

For Ni$^{3+}$ completely substituted all the Al$^{3+}$ cations of $\gamma$-Al$_2$O$_3$ (110) surface, the substitution reaction of (110)-4Ni-1234 structure is exothermic by $-95$ kJ/mol. It means that the Ni$^{3+}$ cations 100% substitution for the top layer Al$^{3+}$ cations are thermodynamically favorable. In addition, the (110)-4Ni-1234 structure is similar to the 110-4Co-1234 structure. After all the top layer Al$^{3+}$ cations have been substituted, there is no large structural distortion, and 25% Me (one Co$^{3+}$/Ni$^{3+}$) in tetrahedral position vs. 75% Me (three Co$^{3+}$/Ni$^{3+}$) in octahedral position.

Table 1 shows the average Me-O bond distances and average Co/Ni Bader charges of the Co and Ni doped $\gamma$-Al$_2$O$_3$ (110) surfaces. The substitution energies of Co substituted the (110) surface first increases and then decreases with the increase of Co atoms. It due to the Co-O bond distances are shortened and distorted by the (110) surface, especially the Co(2)-O(5) bond distance of 169 pm in the (110)-4Co-1234 structure. More details, it is worth noting that the Al(1) and Al(2), O(2) and O(3), O(5) and O(6) have the same chemical environment in the original $\gamma$-Al$_2$O$_3$ (110) surface. After the Co substitution, the Co(4)-O(5) and Co(4)-O(6), Co(1)-O(6) and Co(2)-O(5), Co(1)-O(3) and Co(2)-O(2) bonds distances are not equal in the (110)-4Co-1234 structure. For the Ni substituted $\gamma$-Al$_2$O$_3$ (110) surface, the Ni(1)-O and Ni(2)-O have the same bond distances in the (110)-4Ni-1234 structure. This results in a higher substitution energy of (110)-4Ni-1234 than (110)-4Co-1234.The average Co-O and Ni-O bond distances are in the range of 181~191 pm and 178~188 pm, respectively, which are slightly longer than the original Al-O bond distances (171~179 pm) of $\gamma$-Al$_2$O$_3$ (110) surface. It is due to the larger covalent radius of Co (126 pm) and Ni (124 pm) than Al (121 pm) [48]. In addition, the Bader charge of substituted Co and Ni are range in +1.39~+1.42 and +1.03~+1.22 e, which are similar to the Bader charges of Co(OH)$_3$ (Co$^{3+}$,

+1.34 e) and $Ni(OH)_3$ ($Ni^{3+}$, +1.16 e), the Mulliken charge of the Fe doped $\gamma$-$Al_2O_3$ (111) surfaces ($Fe^{3+}$, +1.47 e) [28].

**Table 1.** The $E_{sub}$, average Me−O bond distances and average Bader charges of substituted Me atoms for the most stable substituted structures.

| Substituted | $E_{sub}$ (kJ/mol) | Charge (*e*) | Co-O (pm) | Substituted | $E_{sub}$ (kJ/mol) | Charge (*e*) | Co-O (pm) |
|---|---|---|---|---|---|---|---|
| (110)-1Co-4 | −61 | +1.40 | 187 | (110)-1Ni-4 | −57 | +1.22 | 184 |
| (110)-2Co-34 | −83 | +1.42 | 183,191 | (110)-2Ni-34 | −91 | +1.10 | 187,186 |
| (110)-3Co-234 | −67 | +1.42 | 181,191,189 | (110)-3Ni-234 | −96 | +1.03 | 183,188,185 |
| (110)-4Co-1234 | −48 | +1.39 | 184,191,184,189 | (110)-4Ni-1234 | −95 | +1.08 | 178,187,185,185 |

Table 2 collects some Me substituted surfaces. It shows the substitution energy of Co substitution into $\gamma$-$Al_2O_3$ (110) surface is large than Co substitution into the $CuAl_2O_4$ (110) surface. While the substitution energy of the Ni doped $\gamma$-$Al_2O_3$ (110) surface is less than Ni doped into the $CuAl_2O_4$ (110) surface. Moreover, the substitution energies of Me doped $\gamma$-$Al_2O_3$ (110) surface are order of Cu > Co > Ni > Fe.

**Table 2.** The $E_{sub}$ and calculation method of different metals substituted surfaces.

| Substituted | $E_{sub}$ (kJ/mol) | Method | Ref. |
|---|---|---|---|
| Co and Ni doped $\gamma$-$Al_2O_3$ (110) | −61/−57 | GGA-PBE | This work |
| Fe doped $\gamma$-$Al_2O_3$ (111) | −22 | MN12-L | [28] |
| Cu doped $\gamma$-$Al_2O_3$ (110) | −261 | GGA-PBE | [35] |
| Fe doped $\gamma$-$Al_2O_3$ (110) | −53/−52 | GGA-PW91/PBE | [47] |
| Co and Ni doped Al of $CuAl_2O_4$ (110) | −30/−61 | GGA-PBE | [25] |

*2.2. Electronic Structure Analysis*

Using the DFT to study the electronic structure of doped surface could easily provide doping mechanism of active metals and support surfaces. The PDOS of perfect and Me doped $\gamma$-$Al_2O_3$ (110) surfaces top layer are shown in Figure 3. For the Co atoms substituted $\gamma$-$Al_2O_3$ (110) surface, it can be seen the occupied Co 3d orbital overlaps with O 2p orbital. It is worth noting that the band gap of the perfect $\gamma$-$Al_2O_3$ (110) surface is 3.3 eV [41], while the band gap for the $\gamma$-$Al_2O_3$ (110) surface after Co doping becomes narrower. For the four Co substituted, the band gap of (110)-4Co-1234 surface is 0.8 eV, which is 2.5 eV narrower than the perfect $\gamma$-$Al_2O_3$ (110) surface. For the Ni atoms substitute $\gamma$-$Al_2O_3$ (110) surface, the PDOS of Ni substituted (110) surface shows similar characters with Co substitute surface. The interaction mechanism for substituted Ni cations is the interaction of Ni 3d orbital with surface O 2p orbital. The band gap for (110)-4Ni-1234 is 0.4 eV. In addition, the band gaps change and become narrower as the increased of doping, which is consistent with the Fe and Cu substituted $\gamma$-$Al_2O_3$ surfaces [35,47], Fe and Cr substituted $\alpha$-$Al_2O_3$(0001) surface [30].

Moreover, the experimental detection difficult to characterize electronic information of a given surface, the results of PDOS could provide theoretical data for comparison with experiments. The PDOS curves could facilitate characterize and compare the Lewis acidity of catalysts. In this study, the unoccupied 4s and 3d orbital of the substituted Co and Ni atoms are close to the Femi level, which could work as Lewis acid site. It can obviously change the catalytic performance. For example, the different sites of Fe and Cr doped $\alpha$-$Al_2O_3$(0001) surface had different CO adsorption ability reported by Baltrusaitis et al. [30].
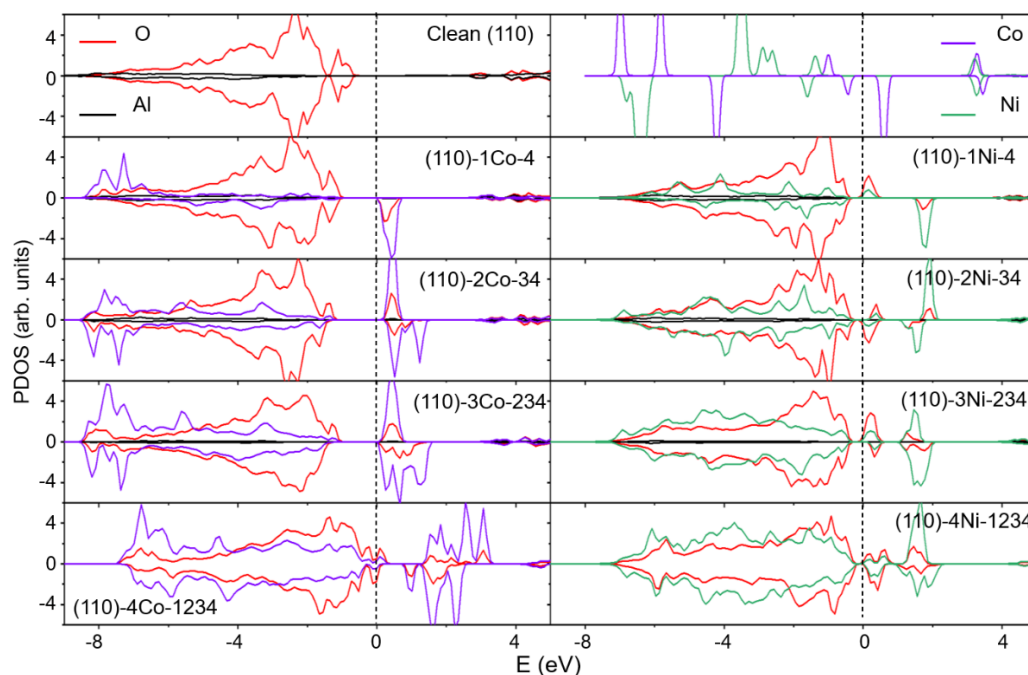
**Figure 3.** PDOS curves for gas phase Co and Ni atom, perfect and metal substituted γ-Al$_2$O$_3$ (110) surfaces.

### 2.3. Thermodynamic Properties

2.3.1. Substitution Reaction under Given Conditions

The free energy change is used to investigate the thermodynamic properties of substitution reaction under the doped catalyst preparation conditions in forma (3). The corresponding function of substitution reaction free energy change (Δ*G*) of *n* and α(Al$^{3+}$)/[α(Me$^{3+}$)] under given temperature is expressed by Equation (1). Where the G[Al$_{(4-n)}$(Me)$_n$O$_6$*] and G(Al$_4$O$_6$*) are the Δ*G* of the perfect and Me doped γ-Al$_2$O$_3$ (110) surface, respectively. The α(Al$^{3+}$) and α(Me$^{3+}$) are the activity of Al$^{3+}$ and Me$^{3+}$ in solution, respectively.

$$\Delta G = G[Al_{(4-n)}(Me)_nO_6^*] + nG[Al(OH)_3] - G(Al_4O_6^*) - nG(Me(OH)_3)] + RT \times \ln[\alpha(Al^{3+})/\alpha(Me^{3+})]^n, \tag{1}$$

Figure 4 illustrates the function of substitution reaction free energy change (Δ*G*) of ln[α(Al$^{3+}$)/α(Me$^{3+}$)] under 300 K. It can be found that the substitution reaction of Co and Ni substitution into the γ-Al$_2$O$_3$ (110) surface is thermodynamically favored at 300 K. For the Co$^{3+}$ cations substitution into the (110) surface, Co could form 100% (n = 4) substitution for γ-Al$_2$O$_3$ (110) surfaces top layer Al atoms when the value of ln[α(Al$^{3+}$)/α(Co$^{3+}$)] is lower than 114. When the value of ln[α(Al$^{3+}$)/α(Co$^{3+}$)] is higher than 114, the substitution reaction of Al$^{3+}$ substitution by Co$^{3+}$ cannot occur. For the Ni$^{3+}$ cations substitution into (110) surface, all the surface Al$^{3+}$ cations (n = 4) could be doped with the value of ln[α(Al$^{3+}$)/α(Ni$^{3+}$)] lower than 163 vs. ln[α(Al$^{3+}$)/α(Ni$^{3+}$)] higher than 163 the substitution reaction cannot occur.

It is worth noting that Ni$^{3+}$ cations are more easily substituted into the (110) surface Al$^{3+}$ cations than the Co$^{3+}$ cations under the temperature of 300 K.
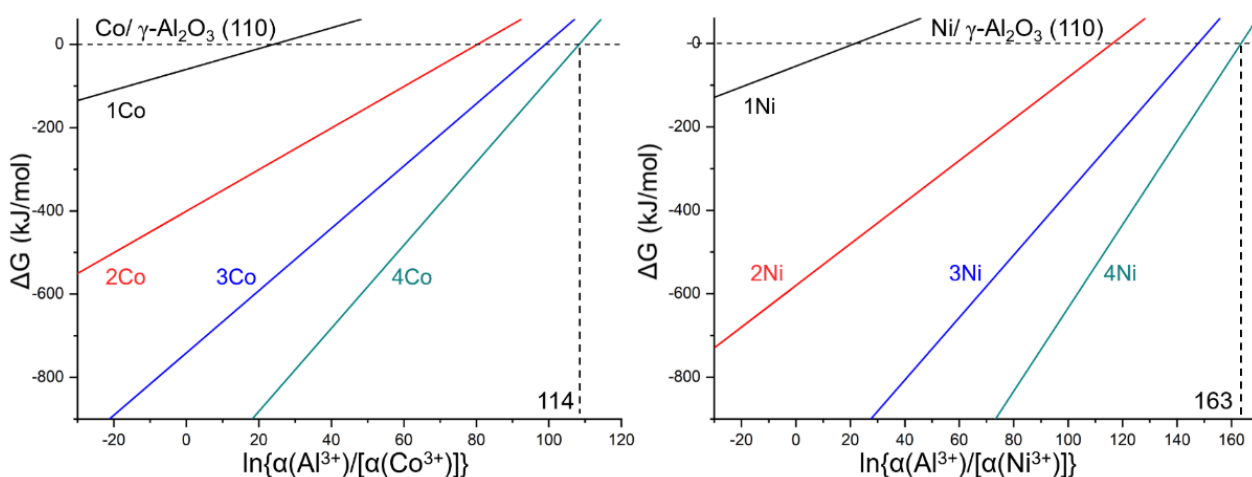
**Figure 4.** The function of substitution reaction free energy change ($\Delta G$) of $\ln[\alpha(Al^{3+})/\alpha(Me^{3+})]$ under 300 K in the Equation (3).

### 2.3.2. Surface O-Defects of the Co and Ni Substituted Surfaces

Surface oxygen vacancy is a typical state of oxide catalysts, which can affect the stability and performance of catalysts. In this part, oxygen vacancy formation energy was employed to explore the stability of the Co and Ni substituted $\gamma$-Al$_2$O$_3$ (110) surface. In the Equation (2), the $E(O_2)$, $E[(Me)_4O_5^*]$ and $E[(Me)_4O_6^*]$ are the total energies of the isolated gas-phase O$_2$ molecule, O-defective surface, and four Ni and Co substituted $\gamma$-Al$_2$O$_3$ (110) surfaces, respectively.

$$E_f = E[(Me)_4O_5^*] + 1/2E(O_2) - E[(Me)_4O_6^*], \qquad (2)$$

Each oxygen atom was calculated to detect the most stable O-defective surface structure. The most stable one O-defective Ni and Co substituted $\gamma$-Al$_2$O$_3$ (110) surfaces have been shown in Figure 5. The computational results show that the O(5)$_{3c}$ is the preferred thermodynamically favorable that could be removed from the surface to form (110)-4Co-1234-dO5 structure, with the oxygen vacancy formation energy of 268 kJ/mol. After the removal of O(5)$_{3c}$ atom, the O(6)$_{3c}$ becomes tri-coordinated. The O(6)$_{3c}$ bonds with Co(1,2,4) with the bond distances are 191, 201 and 183 pm, respectively. For the (110)-4Co-1234 surface, the thermodynamically favorable O-defective site is O(5)$_{3c}$, which has the same structure with (110)-4Co-1234-dO5. The oxygen vacancy formation energy of (110)-4Ni-1234-dO5 is 53 kJ/mol, which is lower than the (110)-4Co-1234-dO5 by 215 kJ/mol. Compared with other surfaces, the oxygen vacancy formation energy of the Co and Ni doped $\gamma$-Al$_2$O$_3$ (110) surfaces are lower than the Cu doped $\gamma$-Al$_2$O$_3$ (110) surface (367 kJ/mol). In addition, it reports that the oxygen vacancy formation energy of Co$_3$O$_4$ (110) [51], Co$_3$O$_4$ (110) [52], NiO (100) [53] are 59, 4 and 424 kJ/mol, respectively.
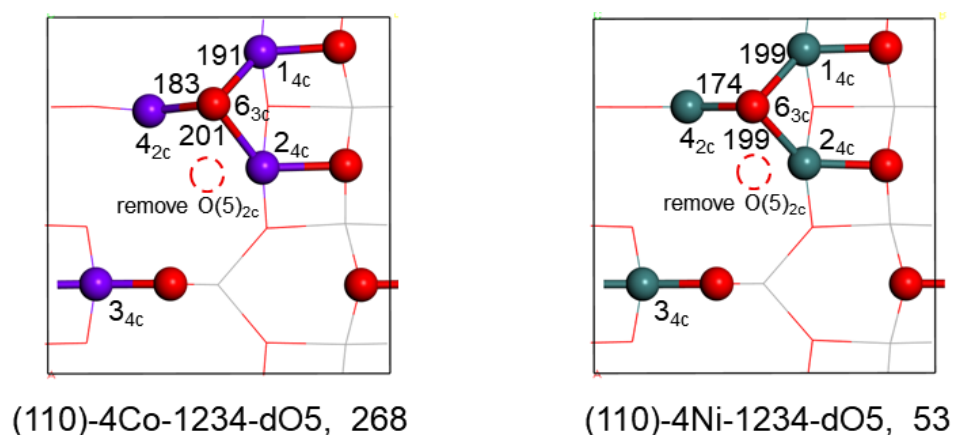
**Figure 5.** The structures for (110)-4Co-12345 and (110)-4Ni-12345 with one O defect. The dotted circle represents the removed O atom.

### 3. Computation Details

*3.1. Computational Methods*

The PBE functional was used for the present work, since we want to compare the results of the present work with our previous works on the NiCu-alumina [35,54], as well as other catalytic works on the alumina [55,56], Fe-alumina [28,47], Co-alumina [57], Ni-alumina [58], Cu-alumina [59,60], Ag-alumina [34], Pt-alumina [61,62] and Pd-alumina [63]. It had been proved that the PBE and PW91 functional work well for such systems for discussions on the reaction, adsorption and substitution energies.

All calculations were performed using the DFT with D3 dispersion correction [64] method with the GGA-PBE [65] functional in the Vienna ab initio Simulation Package [66,67]. Using the projector augmented wave (PAW) method report by Blöchl et al. [68,69] to express the interactions of electron-ion. All calculations are spin-polarized. Using DFT+U methods to correct the strong on-site Coulomb interaction of the Co and Ni 3*d* electrons with the U of 4.0 and 3.8. The Brillouin zone via the Monkhorst–Pack algorithm generated for the unit cell and surface slabs are $5 \times 5 \times 5$ and $3 \times 3 \times 1$ *k*-points meshes, respectively. All calculations were performed using the kinetic energy cutoff of 400 eV. The SCF energy, the total energies and the atomic forces are $1.0 \times 10^{-5}$ eV, $1.0 \times 10^{-4}$ eV and 0.03 eV/Å as the convergence criteria for structure optimizations. The 15 Å $\times$ 15 Å $\times$ 15 Å cell was used to calculate the gas phase molecules.

All reported most stable structures have only one true frequency. The structure vibration frequency is used to calculate the Gibbs free energy, including the oscillator, standard harmonic, ideal gas approximation and rigid rotor. The Gibbs free energy of solid phase surface slabs only consider the vibration contributions. The Gibbs free energy of gas phase substances considers vibration, rotation and translation contributions. In addition, the Bader charge [70] was used to determine the atoms charges.

The substitution reaction of Co and Ni substitution into the $\gamma$-$Al_2O_3$ (110) surface can be considered as Equation (3). Using $Co(OH)_3$ and $Ni(OH)_3$ instead of $Co^{3+}$ and $Ni^{3+}$ cations could more realistically represent Me substitution reaction in solution.

$$n\text{Me(OH)}_3 + \text{Al}_4\text{O}_6{}^* \rightarrow \text{Al}_{(4-n)}(\text{Me})_n\text{O}_6{}^* + n\text{Al(OH)}_3, \tag{3}$$
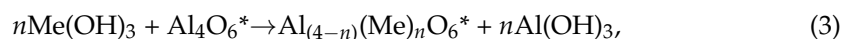
The substitution energy of Me atoms substitute the (110) surface in the Equation (3) is defined as:

$$E_{\text{sub}} = E[\text{Al}_{(4-n)}(\text{Me})_n\text{O}_6{}^*] + nE[\text{Al(OH)}_3] - nE[\text{Me(OH)}_3] - E(\text{Al}_4\text{O}_6{}^*), \tag{4}$$

where the $E[\text{Al(OH)}_3]$ and $E[\text{Me(OH)}_3]$ are the total energies of gas phase $Al(OH)_3$ and $Me(OH)_3$. The $E[\text{Al}_{(4-n)}(\text{Me})_n\text{O}_6{}^*]$ and $E[\text{Me(OH)}_3]$ are the energies of perfect and Me

doped $\gamma$-Al$_2$O$_3$ (110) surfaces. The larger negative of the substitution energy, the more thermodynamics favorable for the substitution reaction in the Equation (3).

### 3.2. $\gamma$-Al$_2$O$_3$ Surface Model

The $\gamma$-Al$_2$O$_3$ (110) surface structure [41,42] was chosen as the calculation model. As shown in Figure 6, all calculations used an eight-layer slab structure. The top and bottom four layers were relaxed and fixed during structural optimization, respectively. In the $\gamma$-Al$_2$O$_3$ (110) surface, the top layer contains Al(1)$_{4c}$, Al(2)$_{4c}$, Al(3)$_{4c}$ and Al(4)$_{3c}$, where the coordination numbers are tetra-coordination and tri-coordination. For surface O atoms, the O(1,2,3)$_{3c}$ and O(4,5,6)$_{2c}$ are in tri- and di-coordinated, respectively. Especially, part surface atoms have the same chemical environment, and for Al atoms are Al(1)$_{4c}$ and Al(2)$_{4c}$, while for O atoms are O(5)$_{2c}$ and O(6)$_{2c}$. In addition, the Al(5)$_{3c}$ is the sublayer Al atom.
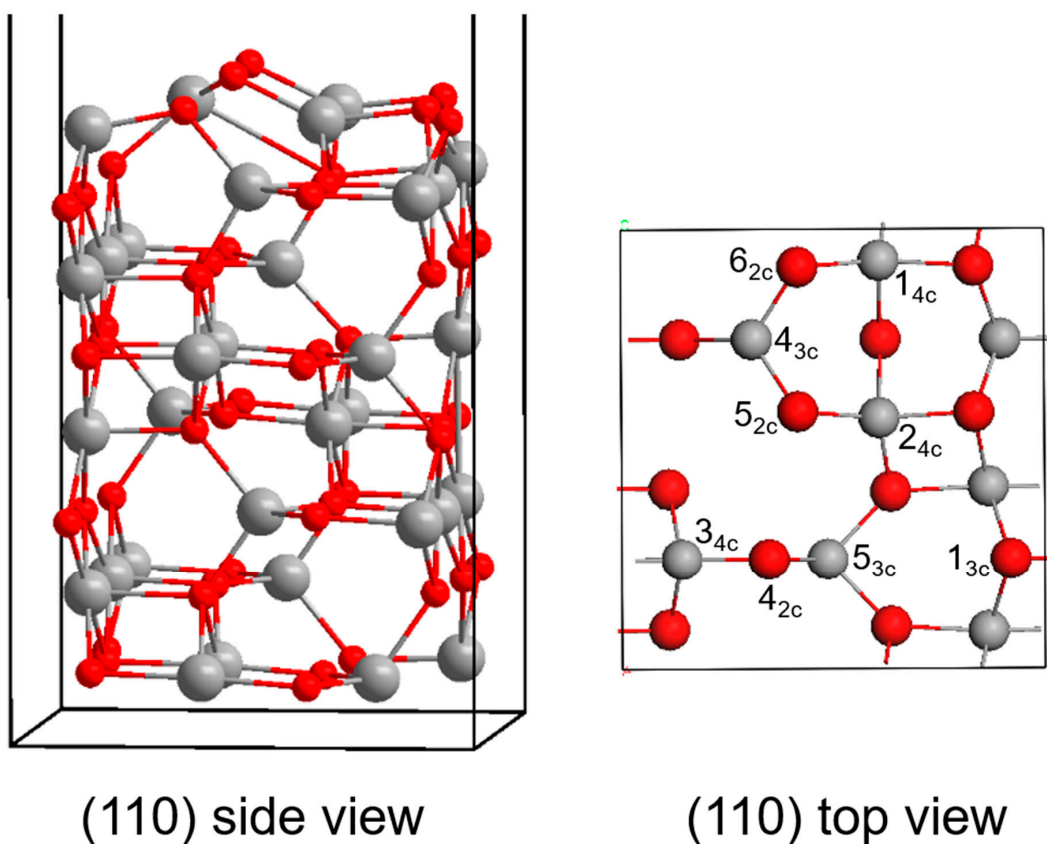


(110) side view          (110) top view

**Figure 6.** The side and top views of $\gamma$-Al$_2$O$_3$ (110) surface. The red and gray balls represent the surface O and Al atoms, respectively. The surface atoms are indexed by numbers. The surface O and Al atoms coordination numbers are shown by subscript numbers.

All the surface Al$^{3+}$ sites substituted by Co$^{3+}$ and Ni$^{3+}$ have been considered, as well as different magnetic moments of Co and Ni atoms. The most thermodynamically stable structure was shown and discussed. The Co and Ni substituted surface structures are identified as '(110)-nMe-p, q'. The name indicates that n Me (Co and Ni) doped for the Al(p) atoms of (110) surface, with the substitution energy of (110)-nMe-p structure is q kJ/mol. Such as the '(110)-2Co-12, 80' means that two Co$^{3+}$ cations substitute the Al(1) and Al(2) atoms. The substitution energy of (110)-2Co-12 structure is 80 kJ/mol. At the same time, the substituted Co$^{3+}$ cations are named Co(1) and Co(2).

## 4. Conclusions

In this work, DFT+U method was performed to investigate the surface properties of the Co and Ni substituted $\gamma$-$Al_2O_3$ (110) surface.

In conclusion, the substitution of $Co^{3+}$ and $Ni^{3+}$ cations for $Al^{3+}$ cations of $\gamma$-$Al_2O_3$ (110) surface are thermodynamically favorable. The substitution energies of one $Al^{3+}$ substitution by $Co^{3+}$ and $Ni^{3+}$ are $-61$ and $-57$ kJ/mol, respectively. The order of substitution site is: $Al_{3c} > Al_{4c}$, as well as preferentially substituting the tetrahedral Al than the octahedral Al atom. Moreover, the substitution of sublayer $Al^{3+}$ cation is thermodynamically unfavorable. After all the top layer $Al^{3+}$ cations have been substituted, there is no large structural distortion, and 25% Me (one $Co^{3+}$/$Ni^{3+}$) in tetrahedral position vs. 75% Me (three $Co^{3+}$/$Ni^{3+}$) in octahedral position.

The interaction mechanism for the substituted $Me^{3+}$ cations and $\gamma$-$Al_2O_3$ (110) surface is Me 3d orbital overlaps with surface O 2p orbital. The surface electronic structure is redistributed after the Co and Ni substitution. The band gap of doped surface is narrower than the perfect $\gamma$-$Al_2O_3$ surface, and become narrower while more $Me^{3+}$ cations is substituted into the surface. The band gap of (110)-4Co-1234 and (110)-4Ni-1234 are 0.8 and 0.4 eV, respectively. The unoccupied 4*s* and 3*d* orbitals of the substituted $Co^{3+}$ and $Ni^{3+}$ cations are close to the Femi level, which could be used as Lewis acid sites.

In addition, the function of substitution reaction free energy change of $\ln[\alpha(Al^{3+})/\alpha(Me^{3+})]$ has been investigated using thermodynamics. It is found that both Co and Ni could form 100% substitution of top layer Al atoms in $\gamma$-$Al_2O_3$ (110) surfaces. Furthermore, the oxygen vacancy formation energies of (110)-4Co-12345 and (110)-4Ni-12345 are 268 and 53 kJ/mol, respectively.

Our work predicts the surface properties of transition metals Co and Ni substitution into the $\gamma$-$Al_2O_3$ (110) surface, providing the molecular level surface structure, doping mechanism and electronic structure characteristic. The calculation results would benefit to design of new high-performance metal doping catalysts.

**Author Contributions:** Investigation, writing—original draft, visualization, H.L.; writing—review and editing, validation, methodology, L.S.; data curation, formal analysis, C.J.; project administration, software, methodology, R.Y.; conceptualization, methodology, resources, supervision, funding acquisition, R.Z. All authors have read and agreed to the published version of the manuscript.

**Data Availability Statement:** Not applicable.

**Conflicts of Interest:** The authors declare no conflict of interest.

## References

1. Weitkamp, J.; Sing, K.S.W.; Schüth, F. *Handbook of Porous Solids*; Wiley-Vch: Weinheim, Germany, 2002; Volume 3, pp. 1543–1591.
2. Ma, W.; Jacobs, G.; Das, T.K.; Masuku, C.M.; Kang, J.; Pendyala, V.R.R.; Davis, B.H.; Klettlinger, J.L.S.; Yen, C.H. Fischer–Tropsch synthesis: Kinetics and water effect on methane formation over 25%Co/$\gamma$-$Al_2O_3$ Catalyst. *Ind. Eng. Chem. Res.* **2014**, *53*, 2157–2166. [CrossRef]
3. Jacobs, G.; Patterson, P.M.; Zhang, Y.; Das, T.; Li, J.; Davis, B.H. Fischer–Tropsch synthesis: Deactivation of noble metal-promoted Co/$Al_2O_3$ catalysts. *Appl. Catal. A* **2002**, *233*, 215–226. [CrossRef]
4. Jacobs, G.; Chaney, J.A.; Patterson, P.M.; Das, T.K.; Davis, B.H. Fischer–Tropsch synthesis: Study of the promotion of Re on the reduction property of Co/$Al_2O_3$ catalysts by in situ EXAFS/XANES of Co K and Re $L_{III}$ edges and XPS. *Appl. Catal. A* **2004**, *264*, 203–212. [CrossRef]
5. Xiong, H.; Zhang, Y.; Wang, S.; Li, J. Fischer–Tropsch synthesis: The effect of $Al_2O_3$ porosity on the performance of Co/$Al_2O_3$ catalyst. *Catal. Commun.* **2005**, *6*, 512–516. [CrossRef]
6. Hu, D.; Gao, J.; Ping, Y.; Jia, L.; Gunawan, P.; Zhong, Z.; Xu, G.; Gu, F.; Su, F. Enhanced investigation of CO methanation over Ni/$Al_2O_3$ catalysts for synthetic natural gas production. *Ind. Eng. Chem. Res.* **2012**, *51*, 4875–4886. [CrossRef]
7. Zhu, X.; Huo, P.; Zhang, Y.-P.; Cheng, D.-G.; Liu, C.-J. Structure and reactivity of plasma treated Ni/$Al_2O_3$ catalyst for $CO_2$ reforming of methane. *Appl. Catal. B* **2008**, *81*, 132–140. [CrossRef]

8.    Dissanayake, D.; Rosynek, M.P.; Kharas, K.C.; Lunsford, J.H. Partial oxidation of methane to carbon monoxide and hydrogen over a Ni/Al$_2$O$_3$ catalyst. *J. Catal.* **1991**, *132*, 117–127. [CrossRef]

9.    Alberton, A.L.; Souza, M.M.; Schmal, M. Carbon formation and its influence on ethanol steam reforming over Ni/Al$_2$O$_3$ catalysts. *Catal. Today* **2007**, *123*, 257–264. [CrossRef]

10.   Comas, J.; Mariño, F.; Laborde, M.; Amadeo, N. Bio-ethanol steam reforming on Ni/Al$_2$O$_3$ catalyst. *Chem. Eng. J.* **2004**, *98*, 61–68. [CrossRef]

11.   Niklasson, G.A.; Granqvist, C.G. Optical properties and solar selectivity of coevaporated Co-Al$_2$O$_3$ composite films. *J. Appl. Phys.* **1984**, *55*, 3382–3410. [CrossRef]

12.   Bechara, R.; Balloy, D.; Vanhove, D. Catalytic properties of Co/Al$_2$O$_3$ system for hydrocarbon synthesis. *Appl. Catal. A* **2001**, *207*, 343–353. [CrossRef]

13.   Bechara, R.; Balloy, D.; Dauphin, J.-Y.; Grimblot, J. Influence of the characteristics of γ-aluminas on the dispersion and the reducibility of supported cobalt catalysts. *Chem. Mater.* **1999**, *11*, 1703–1711. [CrossRef]

14.   Gonçalves, A.A.S.; Costa, M.J.F.; Zhang, L.; Ciesielczyk, F.; Jaroniec, M. One-pot synthesis of MeAl$_2$O$_4$ (Me = Ni, Co, or Cu) supported on γ-Al$_2$O$_3$ with ultralarge mesopores: Enhancing interfacial defects in γ-Al$_2$O$_3$ to facilitate the formation of Spinel structures at lower temperatures. *Chem. Mater.* **2018**, *30*, 436–446. [CrossRef]

15.   Miranda, B.; Chimentao, R.J.; Santos, J.B.; Gispert-Guirado, F.; Llorca, J.; Medina, F.; Bonillo, F.L.; Sueiras, J.E. Conversion of glycerol over 10% Ni/γ-Al$_2$O$_3$ catalyst. *Appl. Catal. B* **2014**, *147*, 464–480. [CrossRef]

16.   Wang, H.; Ruckenstein, E. Conversions of methane to synthesis gas over Co/γ-Al$_2$O$_3$ by CO$_2$ and/or O$_2$. *Catal. Lett.* **2001**, *75*, 13–18. [CrossRef]

17.   Cheng, Z.; Zhao, X.; Li, J.; Zhu, Q. Role of support in CO$_2$ reforming of CH$_4$ over a Ni/γ-Al$_2$O$_3$ catalyst. *Appl. Catal. A* **2001**, *205*, 31–36. [CrossRef]

18.   Hinklin, T.R.; Azurdia, J.; Kim, M.; Marchal, J.C.; Kumar, S.; Laine, R.M. Finding spinel in all the wrong places. *Adv. Mater.* **2008**, *20*, 1373–1375. [CrossRef]

19.   Phillips, B.; Hutta, J.; Warshaw, I. Phase equilibria in the system NiO–Al$_2$O$_3$–SiO$_2$. *J. Am. Ceram. Soc.* **1963**, *46*, 579–583. [CrossRef]

20.   Cava, S.; Tebcherani, S.; Pianaro, S.; Paskocimas, C.; Longo, E.; Varela, J.A. Structural and spectroscopic analysis of γ-Al$_2$O$_3$ to α-Al$_2$O$_3$-CoAl$_2$O$_4$ phase transition. *Mater. Chem. Phys.* **2006**, *97*, 102–108. [CrossRef]

21.   Gassenbauer, Y.; Schafranek, R.; Klein, A.; Zafeiratos, S.; Hävecker, M.; Knop-Gericke, A.; Schlögl, R. Surface states, surface potentials, and segregation at surfaces of tin-doped In$_2$O$_3$. *Phys. Rev. B* **2006**, *73*, 245312. [CrossRef]

22.   Rad, A.S. Adsorption of mercaptopyridine on the surface of Al-and B-doped graphenes: Theoretical study. *J. Alloys Compd.* **2016**, *682*, 345–351.

23.   Harris, J.; Joyce, B.; Dobson, P. Oscillations in the surface structure of Sn-doped GaAs during growth by MBE. *Surf. Sci. Lett.* **1981**, *103*, L90–L96.

24.   Nolan, M. Molecular adsorption on the doped (110) ceria surface. *J. Phys. Chem. C* **2009**, *113*, 2425–2432. [CrossRef]

25.   Li, L.; Gan, Y.-M.; Lu, Z.-H.; Yu, X.H.; Qing, S.; Gao, Z.; Zhang, R.; Feng, G. The effects of Fe, Co and Ni doping in CuAl$_2$O$_4$ spinel surface and bulk: A DFT study. *Appl. Surf. Sci.* **2020**, *521*, 146478. [CrossRef]

26.   Miran, H.A.; Jaf, Z.N.; Altarawneh, M.; Jiang, Z.T. An insight into geometries and catalytic applications of CeO$_2$ from a DFT outlook. *Molecules* **2021**, *26*, 6485. [CrossRef]

27.   Zhang, S.-T.; Li, C.-M.; Yan, H.; Wei, M.; Evans, D.G.; Duan, X. Density functional theory study on the metal–support interaction between Ru cluster and anatase TiO$_2$(101) surface. *J. Phys. Chem. C* **2014**, *118*, 3514–3522. [CrossRef]

28.   Gu, J.; Wang, J.; Leszczynski, J. Single site Fe on the (110) surface of gamma-Al$_2$O$_3$: Insights from a DFT study including the periodic boundary approach. *Phys. Chem. Chem. Phys.* **2021**, *23*, 7164–7177. [CrossRef]

29.   Benam, M.R.; Rahnamaye Aliabad, H.A.; Hosseini, S.M. Effect of substituted IIIB transition metals on the energy gap of α-Al$_2$O$_3$ by first-principle calculations. *Phys. Status Solidi A* **2006**, *203*, 2223–2228. [CrossRef]

30.   Baltrusaitis, J.; Hatch, C.; Orlando, R. Electronic properties and reactivity of simulated Fe$^{3+}$ and Cr$^{3+}$ substituted α-Al$_2$O$_3$ (0001) surface. *J. Phys. Chem. C* **2012**, *116*, 18847–18856. [CrossRef]

31.   Finazzi, E.; Di Valentin, C.; Pacchioni, G. Boron-doped anatase TiO$_2$: Pure and hybrid DFT calculations. *J. Phys. Chem. C* **2009**, *113*, 220–228. [CrossRef]

32.   Yang, S.; Lei, G.; Xu, H.; Xu, B.; Li, H.; Lan, Z.; Wang, Z.; Gu, H. A DFT study of CO adsorption on the pristine, defective, In-doped and Sb-doped graphene and the effect of applied electric field. *Appl. Surf. Sci.* **2019**, *480*, 205–211. [CrossRef]

33.   Zhang, R.; Liu, H.; Wang, B.; Ling, L. Insights into the effect of surface hydroxyls on CO$_2$ hydrogenation over Pd/γ-Al$_2$O$_3$ catalyst: A computational study. *Appl. Catal. B* **2012**, *126*, 108–120. [CrossRef]

34.   Wang, F.; Ma, J.; Xin, S.; Wang, Q.; Xu, J.; Zhang, C.; He, H.; Cheng Zeng, X. Resolving the puzzle of single-atom silver dispersion on nanosized gamma-Al$_2$O$_3$ surface for high catalytic performance. *Nat. Commun.* **2020**, *11*, 529. [CrossRef]

35.   Shi, L.; Huang, Y.; Lu, Z.-H.; Cen, W.; Yu, X.; Qing, S.; Gao, Z.; Zhang, R.; Feng, G. Surface property of the Cu doped γ-Al$_2$O$_3$: A density functional theory study. *Appl. Surf. Sci.* **2021**, *535*, 147651. [CrossRef]

36.   Shibiao, R.; Jinheng, Q.; Chunyan, W.; Bolian, X.; Yining, F.; Yi, C. Influence of nickel salt precursors on the hydrogenation activity of Ni/γ-Al$_2$O$_3$ catalyst. *Chin. J. Catal.* **2007**, *28*, 651–656.

37.   YU, C.-L.; ZHOU, X.-C.; WENG, W.-Z.; HU, J.-B.; Xi-rong, C.; WEI, L.-F. Effects of alkaline-earth strontium on the performance of Co/Al$_2$O$_3$ catalyst for methane partial oxidation. *J. Fuel Chem. Technol.* **2012**, *40*, 1222–1229. [CrossRef]

38. Nagano, T.; Sato, K.; Saitoh, T.; Takahashi, S. Hydrothermal stability of mesoporous Ni-doped γ-Al$_2$O$_3$. *J. Ceram. Soc. Jpn.* **2009**, *117*, 832–835. [CrossRef]

39. Li, H.; Xu, Y.; Gao, C.; Zhao, Y. Structural and textural evolution of Ni/γ-Al$_2$O$_3$ catalyst under hydrothermal conditions. *Catal. Today* **2010**, *158*, 475–480. [CrossRef]

40. Liu, J.; Peng, H.; Liu, W.; Xu, X.; Wang, X.; Li, C.; Zhou, W.; Yuan, P.; Chen, X.; Zhang, W. Tin modification on Ni/Al$_2$O$_3$: Designing potent coke-resistant catalysts for the dry reforming of methane. *ChemCatChem* **2014**, *6*, 2095–2104. [CrossRef]

41. Digne, M. Use of DFT to achieve a rational understanding of acid-basic properties of γ-alumina surfaces. *J. Catal.* **2004**, *226*, 54–68. [CrossRef]

42. Krokidis, X.; Raybaud, P.; Gobichon, A.E.; Rebours, B.; Euzen, P.; Toulhoat, H. Theoretical study of the dehydration process of boehmite to γ-Alumina. *J. Phys. Chem. B* **2001**, *105*, 5121–5130. [CrossRef]

43. Lee, M.H.; Cheng, C.F.; Heine, V.; Klinowski, J. Distribution of tetrahedral and octahedral Al sites in gamma alumina. *Chem. Phys. Lett.* **1997**, *265*, 673–676. [CrossRef]

44. John, C.S.; Alma, N.C.M.; Hays, G.R. Characterization of transitional alumina by solid-state magic angle spinning aluminium NMR. *Appl. Catal.* **1983**, *6*, 341–346. [CrossRef]

45. Zhang, R.; Duan, T.; Wang, B.; Ling, L. Unraveling the role of support surface hydroxyls and its effect on the selectivity of C$_2$ species over Rh/γ-Al$_2$O$_3$ catalyst in syngas conversion: A theoretical study. *Appl. Surf. Sci.* **2016**, *379*, 384–394. [CrossRef]

46. Ja Hun, K.; Jianzhi, H.; Donghai, M.; Cheol-Woo, Y.; Do Heui, K.; Peden, C.H.F.; Allard, L.F.; Janos, S. Coordinatively unsaturated Al$^{3+}$ centers as binding sites for active catalyst phases of platinum on gamma-Al$_2$O$_3$. *Science* **2009**, *325*, 1670–1673.

47. Feng, G.; Huo, C.-F.; Li, Y.-W.; Wang, J.; Jiao, H. Structures and energies of iron promoted γ-Al$_2$O$_3$ surface: A computational study. *Chem. Phys. Lett.* **2011**, *510*, 224–227. [CrossRef]

48. Cordero, B.; Gómez, V.; Platero-Prats, A.E.; Revés, M.; Echeverría, J.; Cremades, E.; Barragán, F.; Alvarez, S. Covalent radii revisited. *Dalton T.* **2008**, *21*, 2832–2838. [CrossRef]

49. Dunitz, J.D.; Orgel, L.E. Electronic properties of transition-metal oxides—I: Distortions from cubic symmetry. *J. Phys. Chem. Solids* **1957**, *3*, 20–29. [CrossRef]

50. Jacob, K.; Alcock, C. Thermodynamics of CuAlO$_2$ and CuAl$_2$O$_4$ and phase equilibria in the system Cu$_2$O-CuO-Al$_2$O$_3$. *J. Am. Chem. Soc.* **2010**, *58*, 192–195. [CrossRef]

51. Zhang, Y.-C.; Pan, L.; Lu, J.; Song, J.; Li, Z.; Zhang, X.; Wang, L.; Zou, J.-J. Unraveling the facet-dependent and oxygen vacancy role for ethylene hydrogenation on Co$_3$O$_4$ (110) surface: A DFT+U study. *Appl. Surf. Sci.* **2017**, *401*, 241–247. [CrossRef]

52. Lu, J.; Song, J.; Niu, H.; Pan, L.; Zhang, X.; Wang, L.; Zou, J.-J. Periodic density functional theory study of ethylene hydrogenation over Co$_3$O$_4$ (1 1 1) surface: The critical role of oxygen vacancies. *Appl. Surf. Sci.* **2016**, *371*, 61–66. [CrossRef]

53. Ferrari, A.M.; Pisani, C.; Cinquini, F.; Giordano, L.; Pacchioni, G. Cationic and anionic vacancies on the NiO(100) surface: DFT+U and hybrid functional density functional theory calculations. *J. Chem. Phys.* **2007**, *127*, 174711. [CrossRef]

54. Li, J.; Shi, L.; Feng, G.; Shi, Z.; Sun, C.; Kong, D. Selective hydrogenation of naphthalene over γ-Al$_2$O$_3$-supported NiCu and NiZn bimetal catalysts. *Catalysts* **2020**, *10*, 1215. [CrossRef]

55. Feng, G.; Huo, C.-F.; Deng, C.-M.; Huang, L.; Li, Y.-W.; Wang, J.; Jiao, H. Isopropanol adsorption on γ-Al$_2$O$_3$ surfaces: A computational study. *J. Mol. Catal. A Chem.* **2009**, *304*, 58–64. [CrossRef]

56. Corral Valero, M.; Raybaud, P.; Sautet, P. Influence of the hydroxylation of γ-Al$_2$O$_3$ surfaces on the stability and diffusion of single Pd atoms: A DFT study. *J. Phys. Chem. B* **2006**, *110*, 1759–1767. [CrossRef]

57. Yang, T.; Ehara, M. Probing the electronic structures of Co$_n$ (n = 1–5) clusters on γ-Al$_2$O$_3$ surfaces using first-principles calculations. *Phys. Chem. Chem. Phys.* **2017**, *19*, 3679–3687. [CrossRef] [PubMed]

58. Pan, Y.-X.; Liu, C.-J.; Ge, Q. Effect of surface hydroxyls on selective CO$_2$ hydrogenation over Ni$_4$/γ-Al$_2$O$_3$: A density functional theory study. *J. Catal.* **2010**, *272*, 227–234. [CrossRef]

59. Thu Ha, N.T.; Minh Hue, V.T.; Trinh, B.C.; Ha, N.N.; Cam, L.M. Study on the adsorption and activation behaviours of carbon dioxide over copper cluster (Cu$_4$) and alumina-supported copper catalyst (Cu$_4$/Al$_2$O$_3$) by means of density functional theory. *J. Chem.* **2019**, *2019*, 4341056. [CrossRef]

60. Feng, G.; Ganduglia-Pirovano, M.V.; Huo, C.-F.; Sauer, J. Hydrogen spillover to copper clusters on hydroxylated γ-Al$_2$O$_3$. *J. Phys. Chem. C* **2018**, *122*, 18445–18455. [CrossRef]

61. Sun, G.; Alexandrova, A.N.; Sautet, P. Pt$_8$ cluster on alumina under a pressure of hydrogen: Support-dependent reconstruction from first-principles global optimization. *J. Phys. Chem. C* **2019**, *151*, 194703. [CrossRef]

62. Mager-Maury, C.; Chizallet, C.; Sautet, P.; Raybaud, P. Platinum nanoclusters stabilized on γ-alumina by chlorine used as a capping surface ligand: A density functional theory study. *ACS Catal.* **2012**, *2*, 1346–1357. [CrossRef]

63. Valero, M.C.; Raybaud, P.; Sautet, P. Nucleation of Pd$_n$ ( n = 1–5 ) clusters and wetting of Pd particles on γ−Al$_2$O$_3$ surfaces: A density functional theory study. *Phys. Rev. B* **2007**, *75*, 045427. [CrossRef]

64. Grimme, S.; Ehrlich, S.; Goerigk, L. Effect of the damping function in dispersion corrected density functional theory. *J. Comput. Chem.* **2011**, *32*, 1456–1465. [CrossRef] [PubMed]

65. Perdew, J.P.; Burke, K.; Ernzerhof, M. Generalized gradient approximation made simple. *Phys. Rev. Lett.* **1996**, *77*, 3865–3868. [CrossRef]

66. Kresse, G.; Furthmüller, J. Efficiency of ab-initio total energy calculations for metals and semiconductors using a plane-wave basis set. *Comput. Mater. Sci.* **1996**, *6*, 15–50. [CrossRef]

67. Kresse, G.; Furthmüller, J. Efficient iterative schemes for ab initio total-energy calculations using a plane-wave basis set. *Phys. Rev. B* **1996**, *54*, 11169–11186. [CrossRef]
68. Blöchl, P.E.; Först, C.J.; Schimpl, J. Projector augmented wave method: Ab initio molecular dynamics with full wave functions. *Bull. Mater. Sci.* **2003**, *26*, 33–41. [CrossRef]
69. Blöchl, P.E. Projector augmented-wave method. *Phys. Rev. B* **1994**, *50*, 17953–17979. [CrossRef]
70. Henkelman, G.; Arnaldsson, A.; Jónsson, H. A fast and robust algorithm for Bader decomposition of charge density. *Comput. Mater. Sci.* **2006**, *36*, 354–360. [CrossRef]